Applied Surface Science 379 (2016) 33–38

Contents lists available at ScienceDirect

Applied Surface Science

journal homepage: www.elsevier.com/locate/apsusc

Preparation of K-doped TiO_2 nanostructures by wet corrosion and their sunlight-driven photocatalytic performance

Eunhye Shin[a,1], Saera Jin[a,1], Jiyoon Kim[a], Sung-Jin Chang[a], Byung-Hyuk Jun[b], Kwang-Won Park[a,*], Jongin Hong[a,*]

[a] Department of Chemistry, Chung-Ang University, Seoul 06974, Republic of Korea
[b] Neutron Science Division, Korea Atomic Energy Research Institute, Daejeon 34057, Republic of Korea

ARTICLE INFO

Article history:
Received 1 January 2016
Received in revised form 28 March 2016
Accepted 30 March 2016
Available online 1 April 2016

Keywords:
Photocatalyst
TiO_2
Wet corrosion
Sunlight
Dye

ABSTRACT

K-doped TiO_2 nanowire networks were prepared by the corrosion reaction of Ti nanoparticles in an alkaline (potassium hydroxide: KOH) solution. The prepared nanostructures were characterized by scanning electron microscopy (SEM), Brunauer-Emmett-Teller (BET) analysis, X-ray photoelectron spectroscopy (XPS), Raman spectroscopy, X-ray diffraction (XRD) and photoluminescence (PL) spectra. Their sunlight-driven photocatalytic activity was also investigated with differently charged dye molecules, such as methylene blue, rhodamine B and methyl orange. The adsorption of the dye molecules on the photocatalyst surface would play a critical role in their selective photodegradation under sunlight illumination.

1. Introduction

Titanium dioxide (TiO_2) has been extensively explored because of its superior photocatalytic activity under UV light irradiation, high chemical stability, and low cost [1–3]. Absorption of photons with energy greater than the bandgap of a semiconductor is conducive for the formation of electrons in the conduction band (CB) and holes in the valence band (VB). If these charge carriers migrate to the semiconductor surface without recombination, they can initiate various redox reactions with adsorbates. Unfortunately, TiO_2 can utilize no more than 5% of the total solar energy impinging on the earth's surface, because of its wide band gap (3.2 eV for anatase, 3.0 eV for rutile, and ~3.2 eV for brookite [4,5]). To cope with this issue, energy band modulation by metal ion doping has been primarily studied with the aim of harnessing a greater amount of solar light for photocatalytic reactions [6]. The incorporation of transition metals and noble metals into the TiO_2 lattice can extend light absorption toward the visible light region, but these metals are very expensive [7,8]. Recently, chemical modification of TiO_2 with alkalis has been proposed to facilitate visible-light absorption [6]. It is reported that alkaline dopants such as Li, Na and K stabilize the anatase phase of TiO_2 and enhance the photocatalytic efficiency under visible light [9–11].

In order to achieve high photocatalytic reaction rates, a large surface area-to-volume ratio is crucial for TiO_2-based photocatalysts. Monodispersed TiO_2 nanoparticles are commonly used since a small crystallite size provides a larger surface area and suppresses electron-hole recombination [12]. Recently, one-dimensional nanostructures (e.g., TiO_2 nanotubes and nanowires) have been suggested to enhance the photocatalytic performance [13]. These nanostructures facilitate efficient charge separation of photogenerated electron-hole pairs and fast transport of such charges to the surface. To date, tubular and fibrous nanostructures have been prepared by numerous methods, including chemical (template) synthesis, electrochemical synthesis, and alkaline hydrothermal method [14–16]. The unique physicochemical properties of TiO_2 render the nanostructures highly promising for various practical applications such as photocatalysis, water splitting, and dye-sensitized solar cells [17,18].

In this study, TiO_2 nanostructures were prepared through a corrosion reaction of Ti nanoparticles in KOH aqueous solutions at room temperature (RT). The photocatalytic activity of the nanostructures under air mass (AM) 1.5 one sun illumination was investigated by using them for the degradation of methylene blue (MB), rhodamine B (RB), and methyl orange (MO), which are cationic, neutral and anionic dyes, respectively.

* Corresponding authors.
E-mail addresses: bryan.kwangwon.park@gmail.com (K.-W. Park), hongj@cau.ac.kr, hong.jongin@gmail.com (J. Hong).
[1] These authors equally contributed to this work.

http://dx.doi.org/10.1016/j.apsusc.2016.03.222
0169-4332/

2. Experimental

2.1. Wet corrosion

Titanium nanoparticles (Ti, diameter ≈70 nm, 99%) were used as the starting material for wet corrosion, and potassium hydroxide (KOH, 95%) was used as a corrosive solution. The photocatalysts were prepared by reacting 1 g of Ti nanoparticles with 20 mL of KOH aqueous solutions (1.0, 5.0, 10.0 and 15.0 mol/L) for 24 h at RT. During the wet corrosion, the mixtures were continuously stirred using a Teflon-coated stir bar and the by-product H_2 was degassed. The wet-corroded particles were thoroughly rinsed with deionized (DI) water and then stored in the DI water for 24 h at RT to remove residual K^+ or OH^- ions on the surface. Subsequently, the particles were collected at the bottom of a centrifuge tube after centrifugation at 7,000 rpm for 10 min and dried on a hot plate at 120 °C for 24 h. Finally, the aggregated samples were ground into fine powders for photocatalytic experiments.

2.2. Characterization

The geometry and morphology of the materials were investigated by field emission scanning electron microscopy (FE-SEM, S-4800, Hitachi). The specific surface area was investigated by Brunauer-Emmett-Teller (BET, Autosorb-iQ 2ST/MP, Quantachrome Instruments) measurement. X-ray photoelectron spectroscopy (XPS) was performed with a K-alpha XPS system (Thermo Fischer Scientific Inc.) using a monochromated Al Kα X-ray source with an energy of 1486.6 eV. The spectra of Ti 2p and O 1s energy levels were calibrated with respect to the C 1s peak at 285.0 eV, attributable to the adventitious carbon formed on the sample surface. Micro-Raman spectroscopy was performed in a back-scattering geometry using a laser operating at a wavelength of approximately 473 nm and a NTEGRA Spectra spectrometer (NT-MDT) with a spectral resolution of 0.7 cm^{-1}. The Raman signals were detected using a Newton electron multiplying charge-coupled device (EMCCD) camera (Andor). The powder X-ray diffraction (PXRD) patterns were collected on a Bruker D8-Advance diffractometer using Cu Kα radiation with 40 kV and 40 mA at room temperature. The photoluminescence (PL) emission spectra were recorded on a PL spectrometer (iHR320, Horiba Ltd.) with excitation wavelength at 350 nm.

2.3. Photocatalytic activity

Photocatalytic performance was measured in terms of the ability of the catalyst to degrade MB, RB, and MO aqueous solutions. 0.1 g of the wet-corroded Ti nanoparticles was dispersed in 100 mL of each dye solution and then stirred continuously in the dark for 90 min to achieve the adsorption equilibrium for each dye on the catalyst. The resulting solution was irradiated under AM 1.5 one-sun illumination (K3000 LAB, McScience). Samples were periodically withdrawn from the reactor and centrifuged at 2,000 rpm for 3 min and at 10,000 rpm for 10 min. The supernatant was subjected to UV–vis absorption spectroscopy (Optizen 3220 UV-bio, Mecasys) analysis.

3. Results and discussion

Fig. 1 shows SEM images of the nanostructures prepared by the corrosion of the Ti nanoparticles with various KOH aqueous solutions. As-received Ti nanoparticles were spherical, and their sizes were 40–50 nm (Fig. S1 in the Supporting information (SI)). Ti nanoparticles were mildly corroded in 1 M KOH, and their initial shape was retained after the KOH treatment (Fig. 1a). However, higher KOH concentration resulted in the formation of nanowires and porous filiform networks. The increase in KOH concentration allowed for the creation of thicker nanothreads and more aggregated networks. The specific BET surface areas of the nanostructures are summarized in Table 1. The surface area increased markedly with an increase in KOH concentration. For example, the surface area of the wet-corroded Ti in 15 M-KOH was 9 times higher than that of the as-received Ti nanoparticles (17.4 m^2/g). This indicates that such wet corrosion would be beneficial for the formation of highly porous filiform networks.

Table 1
Surface area of the wet-corroded Ti samples in KOH aqueous solutions of various concentrations.

BET	1 M	5 M	10 M	15 M
Surface area (m^2/g)	35.3	70.5	143.5	154.0

Table 2
Binding energies of Ti 2p, O 1s, and K 2p levels in XPS fitting.

(unit: eV)	K 2p		Ti 2p		O 1s		
	$2p_{1/2}$	$2p_{3/2}$	$2p_{1/2}$	$2p_{3/2}$	O—H	adsorptive	Ti—O
1 M	295.7	292.9	464.2	458.4	532.1	531.1	530.0
5 M	295.8	293.0	464.2	458.5	532.4	531.3	530.0
10 M	295.8	293.0	464.2	458.6	532.3	531.1	530.0
15 M	295.6	292.9	464.3	458.6	532.4	531.3	529.9

If Ti nanoparticles are immersed into KOH aqueous solution, the passive TiO_2 layer on the Ti surface partially dissolves because of the corrosive attack of the hydroxyl groups (Eq. (1)). Meanwhile, Ti reacts with the alkaline solution through the following hydration reactions (Eqs. (2)–(4)) [19]. Further hydroxyl attack on hydrated TiO_2 can produce negatively charged hydrates (Eq. (5)). Importantly, potassium ions in the solution combine with the charged hydrates, resulting in the formation of K-Ti-O after dehydration:

$$TiO_2 + OH^- \rightarrow HTiO_3^- \quad (1)$$

$$Ti + 3OH^- \rightarrow Ti(OH)_3^+ + 4e^- \quad (2)$$

$$Ti(OH)_3^+ + e^- \rightarrow TiO_2 \cdot H_2O + \frac{1}{2}H_2 \quad (3)$$

$$Ti(OH)_3^+ + OH^- \rightleftharpoons Ti(OH)_4 \quad (4)$$

$$TiO_2 \cdot nH_2O + OH^- \rightleftharpoons \left[HTiO_3^-\right] \cdot nH_2O \quad (5)$$

The chemical identity of the wet-corroded samples was confirmed by XPS. According to the survey X-ray photoelectron spectra (Fig. S2 in the SI), the samples contain K, Ti, and O; no other elements are detected except for carbon, which may have been derived from sample handling. The normalized intensities of the X-ray photoelectron narrow scan spectra of the K 2p, Ti 2p and O 1s levels are shown in Fig. 2 and the dotted lines below the X-ray photoelectron spectra denote the Lorentzian-fitted curves. The observed binding energies of K 2p, Ti 2p, and O 1s are summarized in Table 2. The whole XPS data were corrected using C 1s at 285.0 eV as a reference. In Fig. 2(a), the binding energy of the K $2p_{3/2}$ level around 293.0 eV is in good agreement with that of the K-doped TiO_2 reported in the literature [20]. Courcot et al. reported that the binding energy of K 2p decreases with an increase in the amount of potassium, due to the loss of its cationic character [20]. In our case, the amount of potassium atoms can be estimated as 1-2 atoms/nm^2 on the surface of the K-doped titania. Furthermore, the relative intensity ratio of K 2p to Ti 2p increased as the KOH concentration increased (0.13, 0.26, 0.32, and 0.35 for 1 M, 5 M, 10 M and 15 M KOH, respectively). This accounts for the increment in potassium incorporation into the TiO_2 lattice. In Fig. 2(b), the binding energy of the Ti $2p_{3/2}$ level is slightly lower than that of bulk TiO_2 reported in the literature (458.6 eV and 458.9 eV for anatase and rutile, respectively) [20,21].

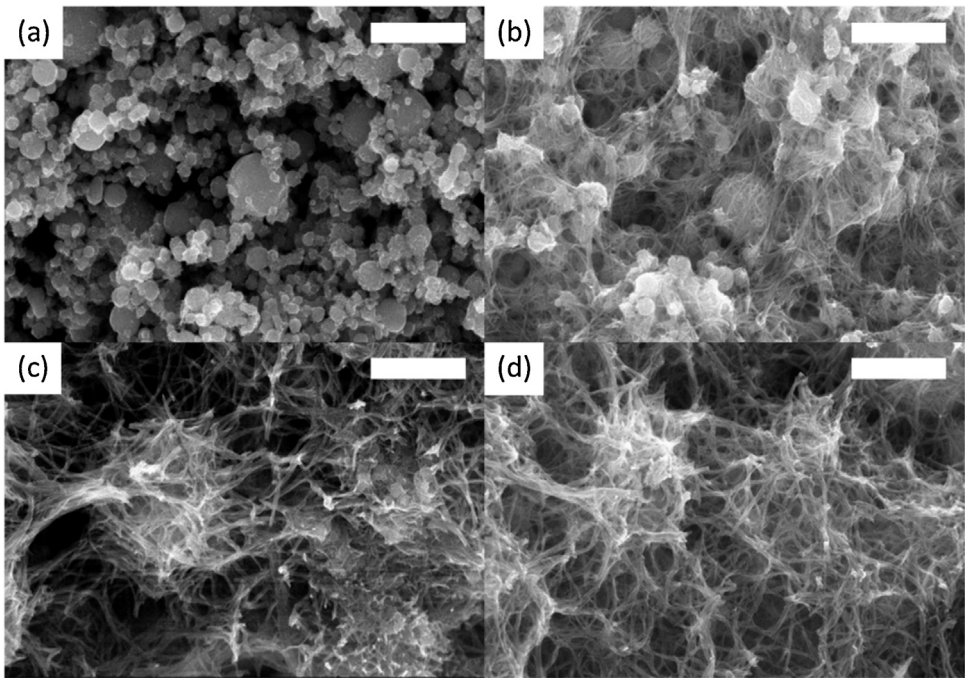

Fig. 1. FE-SEM images of wet-corroded Ti in KOH aqueous solutions of various concentrations: (a) 1 M (b) 5 M (c) 10 M and (d) 15 M for 24 h in RT. Scale bars are 500 nm.

This would result from the change in the oxidation state of some Ti cations from +4 to +3, as the binding energy of Ti^{3+} is lower than that of Ti^{4+} [20]. Such a change in the Ti oxidation state would be related to the incorporation of potassium atoms into Ti—O bonds [20]. In Fig. 2(c), the prominent peak of the O 1s level can be assigned to the Ti—O bond (bulk O^{2-}) in TiO_2 (530.0 eV and 530.5 eV of anatase and rutile, respectively), while the peak at the higher binding energy is related to the hydroxyl groups or oxygen atoms bound to carbon [22]. According to the observed binding energies of the K $2p_{3/2}$, Ti $2p_{3/2}$, and O 1s levels, the prepared photocatalysts can be concluded to be K-doped TiO_2. The Ti nanoparticles corroded with 1 M, 5 M, 10 M, and 15 M KOH solutions are denoted as 1K-TiO_2, 5K-TiO_2, 10K-TiO_2, and 15K-TiO_2, respectively.

Fig. 3 shows the Raman scattering spectra of all the K-TiO_2 samples at RT under approximately 473 nm excitation. Raman spectroscopy is suitable for identifying the anatase and rutile phases of TiO_2. Anatase has the space group $D_{4h}(I4_1/amd)$, with two formula units per unit cell and six Raman active modes ($A_{1g}+2B_{1g}+3E_g$). The six Raman bands of an anatase single crystal were identified at 144 cm^{-1} (E_g), 197 cm^{-1} (E_g), 399 cm^{-1} (B_{1g}), 513 cm^{-1} (A_{1g}), 519 cm^{-1} (B_{1g}), and 639 cm^{-1} (E_g) [23]. In contrast, rutile has the space group $D_{4h}(P4_2/mnm)$, with two units and four Raman active modes ($A_{1g}+B_{1g}+B_{2g}+E_g$). The four Raman bands of a rutile single crystal were identified at 143 cm^{-1} (B_{1g}), 447 cm^{-1} (E_g), 612 cm^{-1} (A_{1g}), and 826 cm^{-1} (B_{2g}) [23]. In addition, the band at 144 cm^{-1} is the strongest for the anatase phase, whilst that at 143 cm^{-1} is the weakest for the rutile phase. In Fig. 3, both 1K-TiO_2 and 5K-TiO_2 samples show distinctive Raman peaks due to the anatase and rutile phases: the broad peaks at ~400 cm^{-1} and ~600 cm^{-1} might originate from the blueshift of the characteristic Raman peaks of anatase at 399 cm^{-1}, 639 cm^{-1}, and those of rutile at 447 cm^{-1}, 612 cm^{-1}, respectively [24]. Thus, it can be concluded that the samples are a mixture of anatase and rutile phases. The shift of the peaks toward lower value as compared with bulk TiO_2 could be attributed to the non-stoichiometry resulting from oxygen deficiency or structural defects, or both [25,26]. It should be noted

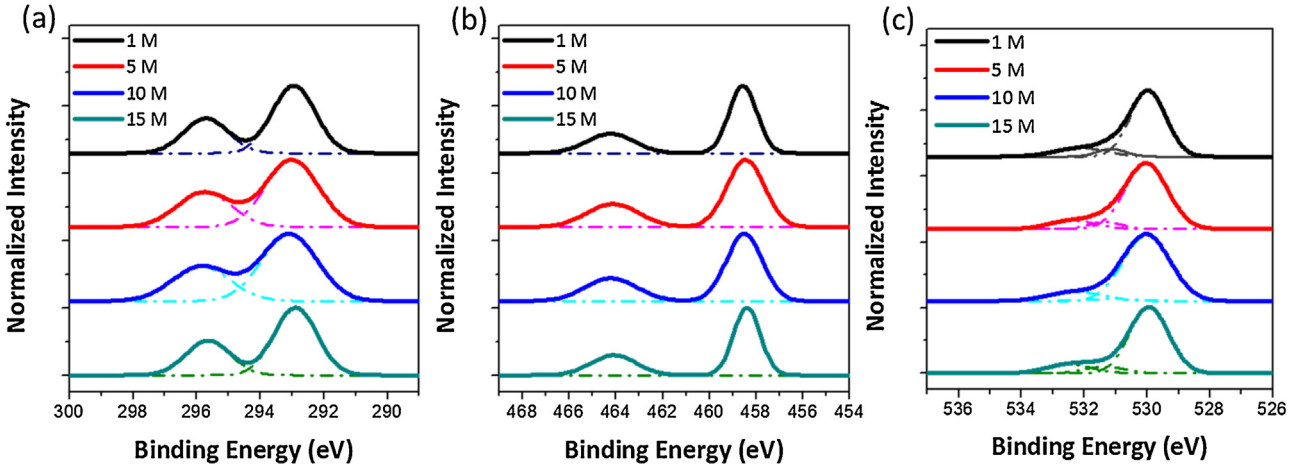

Fig. 2. Normalized intensity of X-ray photoelectron narrow scan spectra for (a) K 2p (b) Ti 2p, and (c) O 1s levels. The dotted line below the X-ray photoelectron spectra denotes the Lorentzian-fitted curves.

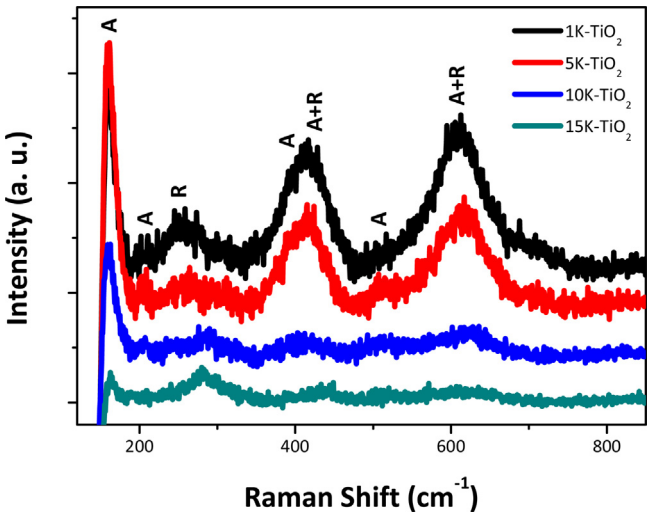

Fig. 3. Raman spectra of all K-TiO_2 samples.

Table 3
Amount of MB adsorption on the prepared photocatalysts.

(Unit. mg/L)	1K-TiO_2	5K-TiO_2	10K-TiO_2	15K-TiO_2
Initial conc.	45.0	55.0	120.0	90.0
Final conc.	20.4	19.9	19.3	20.9
Adsorption	24.6	35.1	100.7	69.1

that the peaks of the anatase phase in 5K-TiO_2 are more intense and sharper than those in 1K-TiO_2. Unfortunately, both 10K-TiO_2 and 15K-TiO_2 show less intense and broader Raman peaks. This indicates poor crystallinity and thus optical phonons may decay at the imperfect sites [27]. In addition, the peaks at 280 and 440 cm^{-1} can be assigned to the Ti-O-K bonding in the potassium titanate structure [28]. The structures of our K-TiO_2 samples were also investigated by the PXRD analysis (Fig. S3 in the SI). All the K-TiO_2 samples showed low-crystalline anatase phase whilst the intensity of crystalline Ti peaks decreased with the increase in the KOH concentration.

In order to evaluate the photocatalytic activity of all the K-TiO_2 samples, photodegradation of MB was performed at RT under AM 1.5 one-sun illumination (Fig. 4). Before the photodegradation experiments, adsorption of the MB molecules on the K-TiO_2 samples was monitored by UV–vis spectroscopy (Fig. S4 in the SI). After stirring the solution for 90 min in dark, adsorption equilibrium was reached. Table 3 summarizes the concentration of the MB solution before the addition of the catalyst and after the adsorption equilibrium. As the KOH concentration for wet corrosion increased, the MB adsorption increased, reached the maximum at 10K-TiO_2, and then decreased. This is analogous to the trend in the specific BET surface area, except for 15K-TiO_2. Interestingly, the K-TiO_2 rapidly and selectively adsorbed the cationic dye, MB. However, no uptake of anionic and neutral dye molecules on the K-TiO_2 surface was observed (Fig. S4(b) and (c) in the SI). Thus, this indicates that the incorporation of K^+ ions into TiO_2 would make the surface become significantly more negative. Fig. 4(a) shows the temporal evolution of the absorption spectra during the photodegradation of MB in aqueous 5K-TiO_2 suspension. It is clearly shown that the MB molecules were gradually decomposed under AM 1.5 one-sun illumination. Normally, the TiO_2-based photocatalyst under UV irradiation generates holes in the VB and electrons in the CB. The photogenerated charge carriers initiate various oxidation and reduction reactions on the photocatalyst surface and decompose the MB molecules [29,30]. However, under sunlight irradiation, photoexcitation of the MB molecules adsorbed on the photocatalyst would occur because MB is an aromatic compound showing maximum light absorption at around 670 nm. This allows for electron transfer from the excited MB molecules to the CB of the photocatalyst or hole transfer from the photogenerated holes to the VB of the photocatalyst, or both. The electrons participate to form superoxide radicals ($^{\circ}O_2^-$) and then hydroperoxyl radicals ($^{\bullet}HO_2$), whilst the holes react with water to produce a hydroxyl radical ($\cdot OH$). These radicals would attack the oxidized dyes, yield intermediate products, and allow for complete mineralization of the MB molecules containing carbon, nitrogen, and sulfur into the final oxidation products (CO_2, NO_3^-, and SO_4^{2-}). Removal of the adsorbed dyes provides vacant adsorption sites for the MB molecules existing in the solution. This series of processes is repeated under sunlight irradiation. Importantly, it is reasonable to postulate that prior adsorption of the dyes on the photocatalyst surface is inevitable for sunlight-driven photodegradation. Fig. 4(b) shows the photocatalytic degradation rate over all the K-TiO_2 samples under AM 1.5 one-sun illumination. 15K-TiO_2 shows the highest degradation rate because it has the largest specific BET surface area among all the samples. However, if the effect of surface area on the photodegradation is eliminated, 15K-TiO_2 would have the lowest photocatalytic activity because of its poor crystallinity and excess K^+ incorporation into TiO_2 lattices [28].

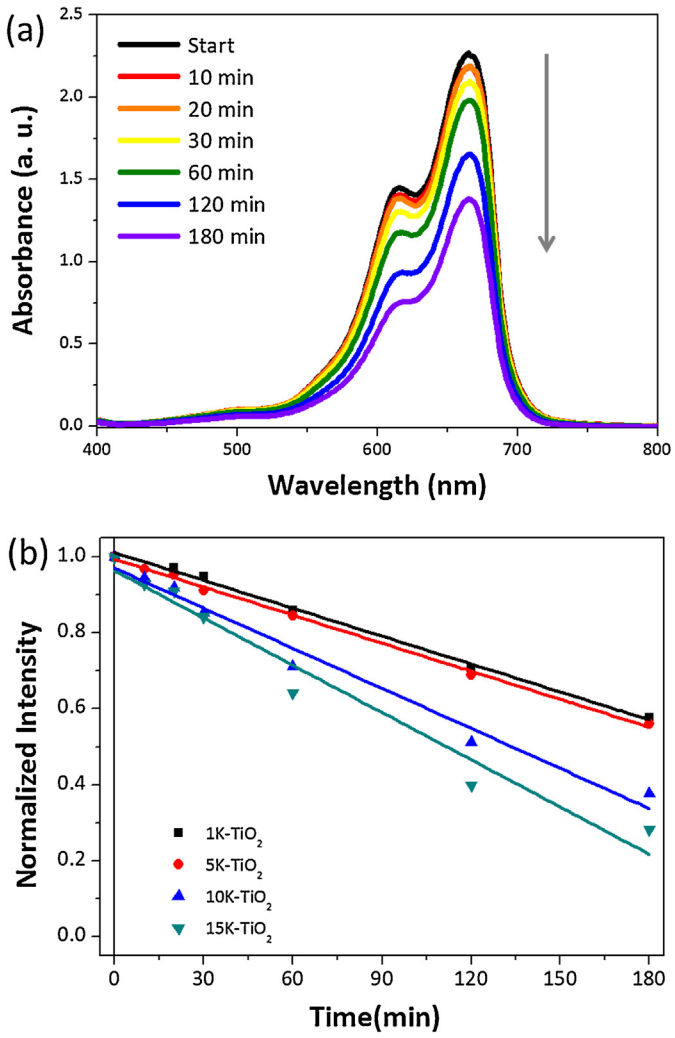

Fig. 4. (a) Temporal evolution of UV–vis absorbance spectra of MB (55 mg/L) aqueous solution with 5K-TiO_2 suspension and (b) rate of photocatalytic degradation over all the K-TiO_2 samples under AM 1.5 one-sun illumination.

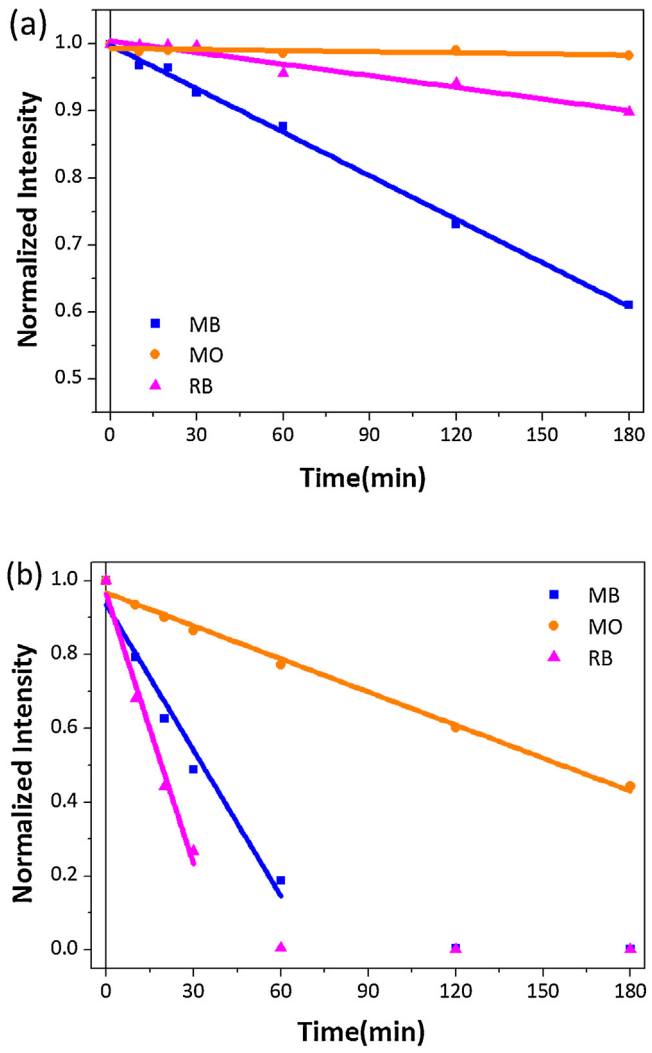

Fig. 5. Photocatalytic degradation rate of MB, RB, and MO with (a) 5K-TiO_2 and (b) P25.

Fig. 5 shows the photocatalytic degradation of MB, RB, and MO, which are cationic, neutral, and anionic dyes, respectively. Intriguingly, the charge on the dye molecules plays a significant role in their sunlight-driven photodegradation. The adsorption of the dye molecules on the 5K-TiO_2 samples was monitored by UV–vis spectra (Fig. S4). After stirring the solution for 90 min in the dark, 63.8% of MB was adsorbed, whilst RB and MO were hardly adsorbed. After 3 h of sunlight irradiation, 40.0% of MB and 10.0% of RB were decomposed, whilst MO was hardly degraded. This indicates that the K-TiO_2 photocatalyst would be effective in selectively removing dye molecules in water due to the electrostatic attraction between the positive charge on the MB molecules and the negative charge on the K-TiO_2 surface. In Fig. 5(b), corresponding performance of Degussa P25 is also given for comparison. After stirring in dark, all dyes were never adsorbed on Degussa P25 (58.9 m^2/g). P25 was found to be favorable for decomposing MB and RB under AM 1.5 one-sun illumination. In addition, PL spectra were obtained to investigate the relationship between PL attributes and photocatalytic activity of the photocatalysts (Fig. S5 in the SI). Both emission spectra of P25 and 5K-TiO_2 are similar to those of solid TiO_6^{8-} complexes due to the charge-transfer transition from Ti^{3+} to oxygen anion and reflect the mixed characteristics of rutile and anatase phases [31–33]. The PL intensity of P25 was higher that of 5K-TiO_2. The PL intensity is associated with the recombination of the photo-generated electron-hole pairs and the shallow traps on surface oxygen vacancies or defects [32,34]. If the PL emission mainly results from the recombination of photo-induced charges, the lower PL intensity indicates fewer recombination between electrons and holes. However, the effect of the oxygen vacancies or defects on the PL intensity cannot be neglected. Depending on their abundance, the sites can become either a separation center or a non-radiative recombination center of photo-induced electrons and holes.

4. Conclusion

The K-doped TiO_2 nanotubular networks were prepared by the corrosion reaction of the Ti nanoparticles in the KOH aqueous solution. Unique nanowire morphologies were obtained corresponding concentration of the KOH solution. Low-crystalline TiO_2 structure could be made at the surface as a result of wet-corrosion process proven by XPS, Raman and XRD. Their sunlight-driven photocatalytic activity was also investigated with the differently charged dye molecules, such as MB, RB and MO. The adsorption of the dye molecules on the photocatalyst surface would be a vital role in their selective photodegradation under AM 1.5 one-sun illumination.

Acknowledgements

This research was supported by the University Research Program through Korea Foundation for the Advancement of Science and Creativity (KOFAC) funded by the Ministry of Education of Korea, the National Research Foundation Grant (NRF-2013M2A8A1035822) from the Ministry of Science, ICT and Future Planning (MSIP) of Korea and the International Cooperative R&D program through Korea Institute for Advancement of Technology (KIAT) funded by the Ministry of Trade, Industry, and Energy (MOTIE) of Korea.

Appendix A. Supplementary data

Supplementary data associated with this article can be found, in the online version, at http://dx.doi.org/10.1016/j.apsusc.2016.03.222.

References

[1] K. Hashimoto, H. Irie, A. Fujishima, TiO_2 photocatalysis: a historical overview and future prospects, Jpn. J. Appl. Phys. 44 (2005) 8269–8285.
[2] B. O'regan, M. Grätzel, A low-cost, high-efficiency solar-cell based on dye-sensitized colloidal TiO_2 films, Nature 353 (1991) 737–740.
[3] X. Chen, S.S. Mao, Titanium dioxide nanomaterials: synthesis, properties, modifications, and applications, Chem. Rev. 107 (2007) 2891–2959.
[4] A.L. Linsebigler, G. Lu, J.T. Yates, Photocatalysis on TiO_2 surfaces: principles, mechanisms, and selected results, Chem. Rev. 95 (1995) 735–758.
[5] M. Koelsch, S. Cassaignon, C. Ta Thanh Minh, J.-F. Guillemoles, J.-P. Jolivet, Electrochemical comparative study of titania (anatase brookite and rutile) nanoparticles synthesized in aqueous medium, Thin Solid Films 451–452 (2004) 86–92.
[6] M. Pelaez, N.T. Nolan, S.C. Pillai, M.K. Seery, P. Falaras, A.G. Kontos, P.S.M. Dunlop, J.W.J. Hamilton, J.A. Byrne, K. O'Shea, M.H. Entezari, D.D. Dionysiou, A review on the visible light active titanium dioxide photocatalysts for environmental applications, Appl. Catal. B: Environ. 125 (2012) 331–349.
[7] X.Z. Li, F.B. Li, Study of Au/Au^{3+}-TiO_2 photocatalysts toward visible photooxidation for water and wastewater treatment, Environ. Sci. Technol. 35 (2001) 2381–2387.
[8] D. Dvoranová, V. Brezová, M. Mazúr, M.A. Malati, Investigations of metal-doped titanium dioxide photocatalysts, Appl. Catal. B: Environ. 37 (2002) 91–105.
[9] L.-C. Chen, C.-M. Huang, F.-R. Tsai, Characterization and photocatalytic activity of K^+-doped TiO_2 photocatalysts, J. Mol. Catal. A: Chem. 265 (2007) 133–140.
[10] Y. Bessekhouad, D. Robert, J.-V. Weber, N. Chaoui, Effect of alkaline-doped TiO_2 on photocatalytic efficiency, J. Photochem. Photobiol. A: Chem. 167 (2004) 49–57.
[11] G. Yang, Z. Yan, T. Xiao, B. Yang, Low-temperature synthesis of alkalis doped TiO_2 photocatalysts and their photocatalytic performance for degradation of methyl orange, J. Alloys Compd. 580 (2013) 15–22.

[12] G. Sivalingam, K. Nagaveni, M.S. Hegde, G. Madras, Photocatalytic degradation of various dyes by combustion synthesized nano anatase TiO_2, Appl. Catal. B: Environ. 45 (2003) 23–38.
[13] Y.-C. Nah, I. Paramasivam, P. Schmuki, Doped TiO_2 and TiO_2 nanotubes: synthesis and applications, Chemphyschem 11 (2010) 2698–2713.
[14] J.-I. Kim, S.-Y. Lee, J.-C. Pyun, Characterization of photocatalytic activity of TiO_2 nanowire synthesized from Ti-plate by wet corrosion process, Curr. Appl. Phys. 9 (2009) e252–e255.
[15] S.-Y. Lee, M. Takai, H.-M. Kim, K. Ishihara, Preparation of nano-structured titanium oxide film for biosensor substrate by wet corrosion process, Curr. Appl. Phys. 9 (2009) e266–e269.
[16] S.-Y. Lee, R. Matsuno, K. Ishihara, M. Takai, Electrical transport ability of nanostructured potassium-doped titanium oxide film, Appl. Phys. Express 4 (2011) 025803.
[17] K.Y. Cheung, C.T. Yip, A.B. Djurišić, Y.H. Leung, W.K. Chan, Long K-doped titania and titanate nanowires on Ti foil and fluorine-doped tin oxide/quartz substrates for solar-cell applications, Adv. Funct. Mater. 17 (2007) 555–562.
[18] C. Xue, X. Xu, G. Yang, S. Ding, Comprehensive investigation of the reciprocity of structure and enhanced photocatalytic performance in finned-tube structured TiO_2/BiOBr heterojunctions, RSC Adv. 5 (2015) 102228–102237.
[19] W. Xiao-jun, Effects of alkali and heat treatment on strength of porous Ti35Nb, Trans. Nonferr. Metals Soc. China 21 (2011) 1335–1339.
[20] D. Courcot, L. Gengembre, M. Guelton, Y. Barbaux, B. Grzybowska, Effect of potassium on the surface potential of titania, J. Chem. Soc. Faraday Trans. 90 (1994) 895–898.
[21] S.O. Saied, J.L. Sullivan, T. Choudhury, C.G. Pearce, A comparison of ion and fast atom beam reduction in TiO_2, Vacuum 38 (1988) 917–922.
[22] D.H. Kim, Z.C. Sun, T.P. Russell, W. Knoll, J.S. Gutmann, Organic-inorganic nanohybridization by block copolymer thin films, Adv. Funct. Mater. 15 (2005) 1160–1164.
[23] J. Zhang, M. Li, Z. Feng, J. Chen, C. Li, UV Raman spectroscopic study on TiO_2. I. Phase transformation at the surface and in the bulk, J. Phys. Chem. B 110 (2006) 927–935.
[24] W. Ma, Z. Lu, M. Zhang, Investigation of structural transformations in nanophase titanium dioxide by Raman spectroscopy, Appl. Phys. A 66 (1998) 621–627.
[25] J.C. Parker, R.W. Siegel, Raman microprobe study of nanophase TiO_2 and oxidation-induced spectral changes, J. Mater. Res. 5 (1990) 1246–1252.
[26] J.C. Parker, R.W. Siegel, Calibration of the Raman spectrum to the oxygen stoichiometry of nanophase TiO_2, Appl. Phys. Lett. 57 (1990) 943–945.
[27] W.F. Zhang, Y.L. He, M.S. Zhang, Z. Yin, Q. Chen, Raman scattering study on anatase TiO_2 nanocrystals, J. Phys. D: Appl. Phys. 33 (2000) 912–916.
[28] C. Liu, X. Lu, G. Yu, X. Feng, Q. Zhang, Z. Xu, Role of an intermediate phase in solid state reaction of hydrous titanium oxide with potassium carbonate, Mater. Chem. Phys. 94 (2005) 401–407.
[29] X. Zhang, J. Yao, D. Li, X. Chen, H. Wang, L.Y. Yeo, J.R. Friend, Self-assembled highly crystalline TiO_2 mesostructures for sunlight-driven, pH-responsive photodegradation of dyes, Mater. Res. Bull. 55 (2014) 13–18.
[30] C. Suwanchawalit, S. Wongnawa, Influence of calcination on the microstructures and photocatalytic activity of potassium oxalate-doped TiO_2 powders, Appl. Catal. A: Gen. 338 (2008) 87–99.
[31] K. Fujihara, S. Izumi, T. Ohno, M. Matsumura, Time-resolved photoluminescence of particulate TiO_2 photocatalysts suspended in aqueous solutions, J. Photochem. Photobiol. A: Chem. 132 (2000) 99–104.
[32] J. Liqiang, Q. Yichun, W. Baiqi, L. Shudan, J. Baojiang, Y. Libin, F. Wei, F. Honggang, S. Jiazhong, Review of photoluminescence performance of nano-sized semiconductor materials and its relationships with photocatalytic activity, Sol. Energy Mater. Sol. Cells 90 (2006) 1773–1787.
[33] J. Yan, G. Wu, N. Guan, L. Li, Z. Li, X. Cao, Understanding the effect of surface/bulk defects on the photocatalytic activity of TiO_2: anatase versus rutile, Phys. Chem. Chem. Phys. 15 (2013) 10978–10988.
[34] B. Lin, C. Xue, X. Yan, G. Yang, G. Yang, B. Yang, Facile fabrication of novel SiO_2/g-C_3N_4 core-shell nanosphere photocatalysts with enhanced visible light activity, Appl. Surf. Sci. 357 (2015) 346–355.